JACS
JOURNAL OF THE AMERICAN CHEMICAL SOCIETY
Article
pubs.acs.org/JACS

Ultrasmall Magnetically Engineered Ag_2Se Quantum Dots for Instant Efficient Labeling and Whole-Body High-Resolution Multimodal Real-Time Tracking of Cell-Derived Microvesicles

Jing-Ya Zhao,[†] Gang Chen,[†,‡] Yi-Ping Gu,[†] Ran Cui,[†] Zhi-Ling Zhang,[†] Zi-Li Yu,[‡] Bo Tang,[†] Yi-Fang Zhao,[‡] and Dai-Wen Pang*[,†]

[†]Key Laboratory of Analytical Chemistry for Biology and Medicine (Ministry of Education), College of Chemistry and Molecular Sciences, State Key Laboratory of Virology, The Institute for Advanced Studies, and Wuhan Institute of Biotechnology, Wuhan University, Wuhan, 430072, P. R. China

[‡]Key Laboratory of Oral Biomedicine (Ministry of Education) and Department of Oral and Maxillofacial Surgery, School and Hospital of Stomatology, Wuhan University, Wuhan, 430079, P. R. China

Supporting Information

ABSTRACT: Cell-derived microvesicles (MVs) are natural carriers that can transport biological molecules between cells, which are expected to be promising delivery vehicles for therapeutic purposes. Strategies to label MVs are very important for investigation and application of MVs. Herein, ultrasmall Mn-magnetofunctionalized Ag_2Se quantum dots (Ag_2Se@Mn QDs) integrated with excellent near-infrared (NIR) fluorescence and magnetic resonance (MR) imaging capabilities have been developed for instant efficient labeling of MVs for their in vivo high-resolution dual-mode tracking. The Ag_2Se@Mn QDs were fabricated by controlling the reaction of Mn^{2+} with the Ag_2Se nanocrystals having been pretreated in 80 °C NaOH solution, with an ultrasmall size of ca. 1.8 nm, water dispersibility, high NIR fluorescence quantum yield of 13.2%, and high longitudinal relaxivity of 12.87 mM^{-1} s^{-1} (almost four times that of the commercial contrast agent Gd-DTPA). The ultrasmall size of the Ag_2Se@Mn QDs enables them to be directly and efficiently loaded into MVs by electroporation, instantly and reliably conferring both NIR fluorescence and MR traceability on MVs. Our method for labeling MVs of different origins is universal and free of unfavorable influence on intrinsic behaviors of MVs. The complementary imaging capabilities of the Ag_2Se@Mn QDs have made the long-term noninvasive whole-body high-resolution dual-mode tracking of MVs in vivo realized, by which the dynamic biodistribution of MVs has been revealed in a real-time and in situ quantitative manner. This work not only opens a new window for labeling with QDs, but also facilitates greatly the investigation and application of MVs.

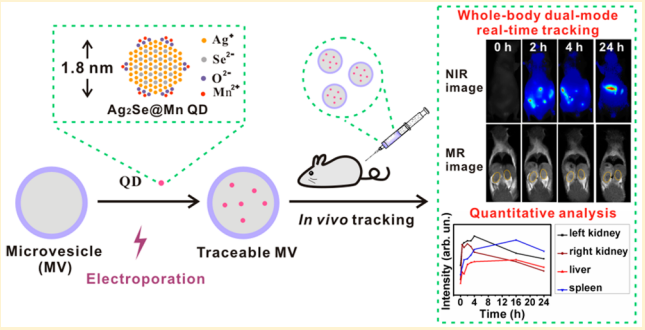

INTRODUCTION

Microvesicles (MVs), also called microparticles or shedding vesicles, are nanosized (100−1000 nm) membrane vesicles released by cells. They bud directly from the plasma membrane and inherit both membrane components and cytoplasmic contents from their donor cells.[1,2] MVs mediate the transfer of bioactive molecules between neighboring or even distant cells, making them important intercellular communicators. They are involved in a number of pathophysiological processes, such as inflammation, tissue repair, and tumor metastasis.[3−6] Notably, recent evidence has indicated that MVs, which naturally function as carriers of biological molecules, are promising delivery vehicles for theranostic purposes.[7−12] Undoubtedly, MVs are becoming a hot topic for both basic and applied studies. However, due to the lack of adequate tracking techniques, current knowledge regarding the tissue distribution and clearance efficiency of MVs in vivo is still deficient, which has severely hampered better understanding and further application of MVs. Therefore, development of a proper labeling and high-resolution imaging strategy that allows clear visualization of the dynamic behaviors of MVs in vivo is highly desirable.

Currently, the main visualization technique for MVs is fluorescence-based imaging. The most commonly used fluorescent materials are organic dyes, fluorescent proteins, and conventional Cd-containing quantum dots (QDs).[13−15] These types of materials mainly emit visible fluorescence and are not good for localizing MVs in vivo due to the high tissue scattering of visible fluorescence. More importantly, the inherent drawbacks of visible fluorescence imaging, such as poor tissue penetration and poor anatomical imaging without adequate spatial information on the target,[16] have severely limited its application in the studies of MVs in vivo. Compared

Received: October 3, 2015
Published: January 23, 2016

ACS Publications © 2016 American Chemical Society

DOI: 10.1021/jacs.5b10340
J. Am. Chem. Soc. 2016, 138, 1893−1903

Scheme 1. Preparation and Application of the Ag_2Se@Mn QDs[a]

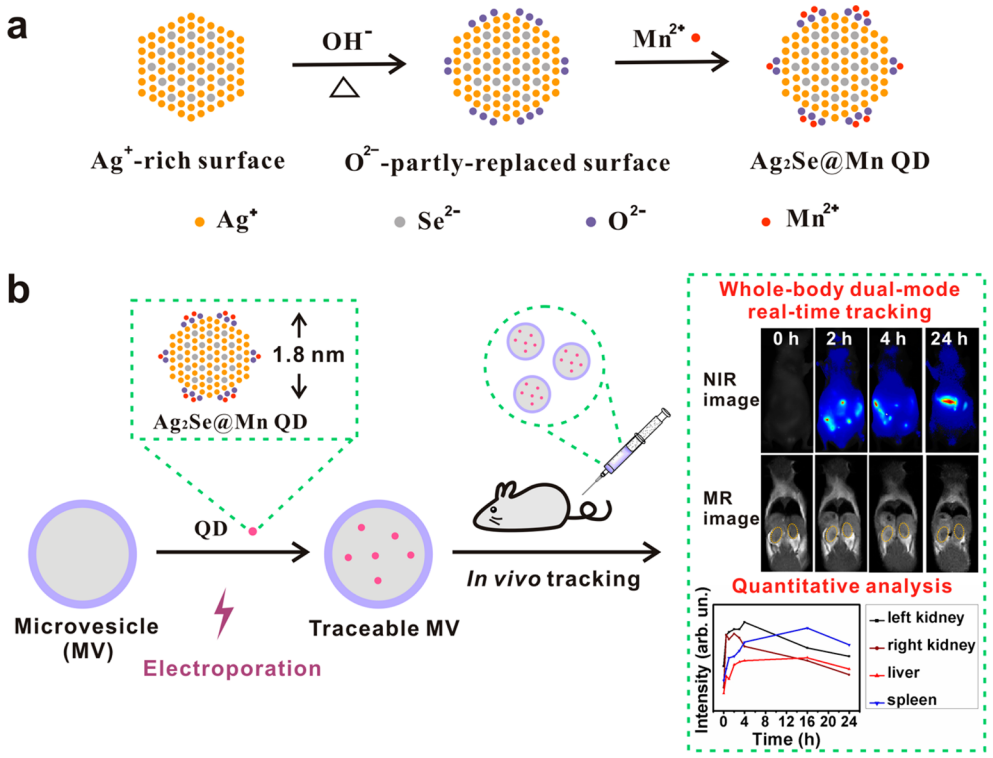

[a](a) Fabrication of the Ag_2Se@Mn QDs by controlling the reaction of Mn^{2+} with the Ag_2Se nanocrystals having been pretreated in 80 °C NaOH solution (0.1 mol/L) for 10 min. (b) Ag_2Se@Mn QD labeling of cell-derived MVs with the assistance of electroporation, and its applications in whole-body high-resolution dual-mode real-time tracking and in situ quantitative analysis of the dynamic bio-distribution of MVs in vivo.

with single fluorescence-based imaging, multimodal imaging is more attractive as it can integrate complementary merits of different imaging modalities to provide more solid information.[17,18] Indeed, several attempts have been made recently to achieve multimodal imaging of MVs. For instance, Lai et al. displayed luciferase and biotin acceptor peptide (for further conjugation with streptavidin-Alexa680) on the donor cell membrane surface via lentiviral vector-mediated stable expression, and then isolated the MVs bearing these biotags, which enabled in vivo bioluminescence and fluorescence imaging of the MVs.[19] Silva et al. incubated the donor cells with magnetic nanoparticles and CdSe QDs, or magnetic nanoparticles and photosensitizer, allowing the internalization of these imaging agents by the donor cells. They then collected the released MVs embedded with both magnetic and optical agents, and realized the combined magnetic resonance (MR) and fluorescence imaging of the MVs in vitro and in vivo.[10,15] Undoubtedly, these strategies for imaging of MVs are significantly advantageous over those of single fluorescence-based imaging. However, several key issues still need to be addressed to achieve a more reliable in vivo high-resolution multimodal tracking of MVs. First of all, because each of the imaging agents used in previous studies has only one imaging capability, multiple agents have to be simultaneously adopted, which means that so far the multimodal imaging of MVs has been based simply on a mixture of different imaging agents. As a result, there is a much heavier burden on such "flimsy" nanosized vesicles. Additionally, different physicochemical properties, such as the stability of mixed agents in intracellular environments, as well as their potential cross-talk and mutual interference, are facing great challenges so as to realize highly synchronous and reliable in vivo multimodal imaging of MVs. Second, currently used optical imaging agents, such as organic dyes and luciferin, suffer from photobleaching and quick clearance in vivo,[20,21] respectively, thus hampering the long-term high-resolution multimodal tracking of MVs in vivo. Third, either the aforementioned labeling materials are too large relative to the nanosized MVs or they are exogenous proteins on the membrane surface of MVs, interfering with the intrinsic behaviors and functions of MVs. In addition, most of the currently used labeling materials, including organic dyes, Cd-containing QDs and virus-mediated biotags, are under suspicion for causing harm to living organisms, thus limiting their in vivo applications.

Considering the above-mentioned facts, we have proposed a strategy to fabricate ultrasmall Mn-magnetofunctionalized Ag_2Se QDs (Ag_2Se@Mn QDs) with integrated near-infrared (NIR) fluorescence and paramagnetism for labeling and tracking MVs. NIR fluorescence imaging is of high sensitivity and deep tissue penetration due to less optical extinction from tissue and blood in the NIR region.[22−28] MR imaging, which is one of the most important tools in clinical diagnostics,[29] can visualize internal anatomical structures with high resolution to provide adequate spatial information about the target. Due to the characteristics of MVs, such as their small size, quick mobility through the circulation, as well as wide distribution in different tissues,[10,19] the methods for the tracking of MVs in vivo are needed with both high spatiotemporal resolution and high identification ability for anatomical structures. Thus, integrating both NIR fluorescence and MR imaging capabilities into a single QD as a multifunctional probe for MV imaging can not only relieve the burden in probe-loading, but also lead to a

DOI: 10.1021/jacs.5b10340
J. Am. Chem. Soc. 2016, 138, 1893−1903

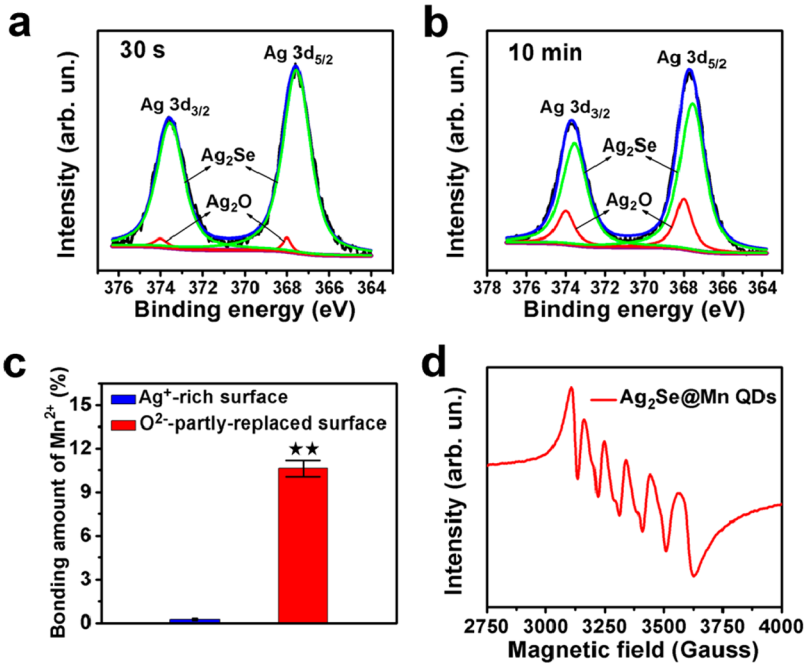

Figure 1. Preparation of the Ag_2Se@Mn QDs. The fitted Ag 3d high-resolution XPS spectra of the Ag_2Se QDs treated for 30 s (a) and 10 min (b) in NaOH solution. The black, green, red, and blue curves in the XPS spectra represent the raw spectra, fitted spectra with two peaks at 367.55 and 373.55 eV, corresponding to Ag 3d in the form of Ag—Se, fitted spectra with two peaks at 368.0 and 374.0 eV, corresponding to Ag 3d in the form of Ag—O, and fitted sum spectra, respectively. (c) ICP-AES analysis of the bonding amount of Mn^{2+} (compared to the total cation amount) for the Ag_2Se QDs with Ag^+-rich surface (control) and O^{2-}-partly replaced surface, ★★, $P < 0.05$ versus the control group. (d) EPR spectrum of the Ag_2Se@Mn QDs.

much better synchronization and complementation of different imaging modalities, acquiring more accurate and reliable information. We fabricated the Ag_2Se@Mn QDs by localizing Mn^{2+} on the surface of the NIR Ag_2Se QDs (Scheme 1a). Such a surface localization of Mn^{2+} can not only preserve the crystal structure of the host Ag_2Se QDs from being changed in their NIR emission, but also enhance NIR emission at 750 nm with a quantum yield of 13.2%, suggesting their promising applicability to in vivo high time-resolution imaging. Moreover, the surface localization of Mn^{2+} enables its direct contact with water, which is in favor of the MR imaging of water protons, thereby leading to a high longitudinal relaxivity (12.87 mM^{-1} s^{-1}, almost four times that of the commercial contrast agent Gd-DTPA) and good performance in MR imaging. In addition, the Ag_2Se@Mn QDs have an extremely small size (ca. 1.8 nm), making them particularly suitable for labeling nanosized MVs because they can avoid undesirable influence on the inherent functions of MVs. Besides their highly integrated dual-mode imaging capabilities and ultrasmall size, the Ag_2Se@Mn QDs do not contain any toxic heavy metal, with superiorities for in vivo applications. Overall, the ultrasmall Ag_2Se@Mn QDs integrated with both strong NIR fluorescence and high longitudinal relaxivity can be anticipated to serve as a novel and advanced biolabeling nanomaterial for in vivo high-resolution multimodal real-time imaging of MVs.

An efficient and biocompatible method to label MVs with the Ag_2Se@Mn QDs is also essential for the reliable high-resolution imaging of MVs, especially in vivo. As aforementioned, a previously reported method for labeling MVs with multiple imaging agents was based simply on incubating the donor cells with different nanoparticles or bioengineering the donor cells to produce biotags, followed by collecting the released MVs from the donor cells. This strategy highly depends on the agent internalization or biotag expression by the donor cells and also on the encapsulation of these agents or biotags into the MVs to be released, which are actually uncontrollable and unreliable. Therefore, this method usually results in a very low labeling efficiency. Moreover, the pretreatment of the donor cells with exogenous nanoparticles or lentiviral vectors may change the intrinsic properties and functions of the resulting MVs because the generation of MVs is a stimulus-sensitive process. Recently, we proposed a reliable and biofriendly membrane biotinylation strategy for labeling the MVs by virtue of the natural membrane phospholipid exchange of their donor cells, with some fascinating advantages.[7] Nevertheless, all of these existing approaches to label MVs depend highly on the assistance of donor cells. Therefore, it is difficult to expand them to labeling of MVs of complex or uncertain origins, such as circulating MVs from body fluids. Electroporation technique, which can instantaneously generate pores of ca. 1−10 nm on the plasma membrane, is commonly used to deliver DNA, RNA, or other small molecules into cells.[30,31] Although electroporation may potentially induce changes in the lipid bilayers, this undesirable effect is negligible in reversible electroporation, which can be easily achieved by controlling the electroporation parameters.[31] MVs are often regarded as miniature versions of cells because they inherit comparable membrane constituents from their donor cells by directly budding from the plasma membrane. By taking advantage of this feature, previous studies, including our recent work, have shown that siRNAs can be quickly and efficiently introduced into MVs by electroporation.[7,32] Further in this work the ultrasmall water-dispersible Ag_2Se@Mn QDs facilitating to go through the instantaneous pores have been directly loaded into the MVs by electroporation to realize instant and efficient labeling of MVs, without tedious pretreatment, chemical modification, and genetic engineering,

DOI: 10.1021/jacs.5b10340
J. Am. Chem. Soc. 2016, 138, 1893−1903

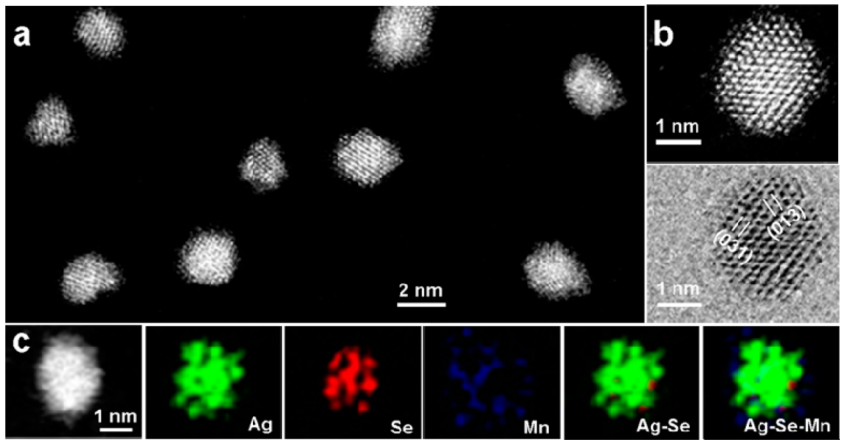

Figure 2. Characterization of the Ag_2Se@Mn QDs. (a) HAADF-STEM image of the Ag_2Se@Mn QDs. (b) High-resolution HAADF-STEM image and the corresponding bright-field image of a single Ag_2Se@Mn QD. (c) STEM-EDX elemental mapping of a single Ag_2Se@Mn QD.

which can maximally maintain the native properties and functions of MVs (Scheme 1b). Such a strategy can also simultaneously confer imaging and therapeutic functions on the MVs. Besides, this labeling method does not need the assistance from donor cells, and thus can be easily used to label a variety of MVs of uncertain origins. On the basis of the MVs labeled with the Ag_2Se@Mn QDs, we have realized the long-term noninvasive whole-body high-resolution dual-mode tracking of MVs in vivo, and revealed the dynamic biodistribution of MVs in a real-time and in situ quantitative manner.

RESULTS AND DISCUSSION

Design and Synthesis of the Ag_2Se@Mn QDs. As depicted in Scheme 1a, the NIR fluorescent-magnetic QD is designed to use the ultrasmall biofriendly NIR Ag_2Se QD as the host material. Mn^{2+} ions as MRI contrast agents are localized on the surface of the QD by controlling the reaction of Mn^{2+} with the Ag_2Se nanocrystal having been pretreated in 80 °C NaOH solution. The surface localization of Mn^{2+} enables its direct contact with water, facilitating the MR imaging of water protons. At the same time, the crystal structure of the host Ag_2Se QDs can also be preserved so that the QDs can maintain their strong NIR emission.

As shown in Figure S1 in the Supporting Information (SI), the ultrasmall Ag_2Se QDs, synthesized by quasi-biosynthesis as we previously reported,[33] were Ag^+-rich. To localize Mn^{2+} on the surface of the host QDs, the Ag^+-rich Ag_2Se was transformed into O^{2-}-partly terminated Ag_2Se by NaOH treatment. X-ray photoelectron spectroscopy (XPS) was used to monitor the transformation of the QD surface composition. As the treatment time increased, the Ag 3d XPS peaks shifted toward high binding energy (Figure S2), implying the formation of Ag—O bonds on the surface of the Ag_2Se QDs. Figure 1, parts a and b, shows the fitted Ag 3d high resolution XPS spectra of the Ag_2Se QDs 30 s and 10 min after NaOH treatment. Typically, the 368.0 and 374.0 eV centered peaks could be assigned to the Ag—O, and 367.55 and 373.55 eV centered peaks were attributed to the Ag—Se. Further quantitative analysis suggested that the percentage of Ag—O on the surface of Ag_2Se QDs gradually increased with the prolonged NaOH treatment (Table S1). All the above results indicated that, upon NaOH treatment, the surface Ag^+ of freshly synthesized Ag_2Se QDs would react with OH^- in the NaOH solution to form Ag_2O on the surface of the QDs. Moreover, the surface Ag_2O content can be controlled by changing the time of NaOH treatment. Therefore, this surface engineering can make the Ag_2Se QDs form the O^{2-}-partly replaced surface. The NaOH treatment time of 10 min was suitable for the subsequent preparation of the Ag_2Se@Mn QDs based on the optimization.

After such a surface engineering, Mn^{2+} can be localized on the surface of the host Ag_2Se QDs via a strong coordination with the surface O^{2-}. In a typical synthesis, Mn^{2+} ions were dropwise added to the solution of surface-engineered Ag_2Se QDs at room temperature. After being stored at 4 °C for 24 h, the QDs were purified by ultrafiltration and dialysis for further characterization. The results from inductively coupled plasma-atomic emission spectroscopy (ICP-AES), and energy-dispersive X-ray spectroscopy (EDX) analyses suggested the successful bonding of Mn^{2+} on the Ag_2Se QDs after the surface engineering (Figure 1c and Figure S3). The bonding amount of Mn^{2+} reached 10.6% (calculated according to the total cation amount). The electron paramagnetic resonance (EPR) spectrum showed a broad six-line pattern, also indicating the presence of Mn^{2+} on the Ag_2Se QDs (Figure 1d). The hyperfine splitting constant calculated from the EPR spectrum can provide the information on the local chemical environment of the Mn^{2+} ions.[34,35] A large hyperfine splitting constant of 93.8 G suggested that, as designed, Mn^{2+} was localized on the surface of the Ag_2Se QDs.[36,37] Such a surface localization of Mn^{2+} was further confirmed by scanning transmission electron microscopy (STEM) analysis. The high-angle annular dark field (HAADF)-STEM images revealed that some elements with relatively low atomic numbers were on the surface of the Ag_2Se@Mn QDs (Figure 2a–c). EDX elemental mapping analysis further showed that Mn^{2+} was present at the surface (Figure 2c), indicating that Mn^{2+} had been localized on the surface of the Ag_2Se@Mn QDs. Moreover, this surface localization of Mn^{2+} did not damage the crystal structure of the host Ag_2Se QDs just as lattice fringes with interplanar distances of 0.23 and 0.24 nm, corresponding to the (031) and (013) planes of Ag_2Se, could still be clearly observed (Figure 2b).

Properties of the Ag_2Se@Mn QDs. The high resolution transmission electron microscopy (HR-TEM) image revealed that the resulting Ag_2Se@Mn QDs were uniform and well-dispersed (Figure 3a). Also, the Ag_2Se@Mn QDs showed an

DOI: 10.1021/jacs.5b10340
J. Am. Chem. Soc. 2016, 138, 1893−1903

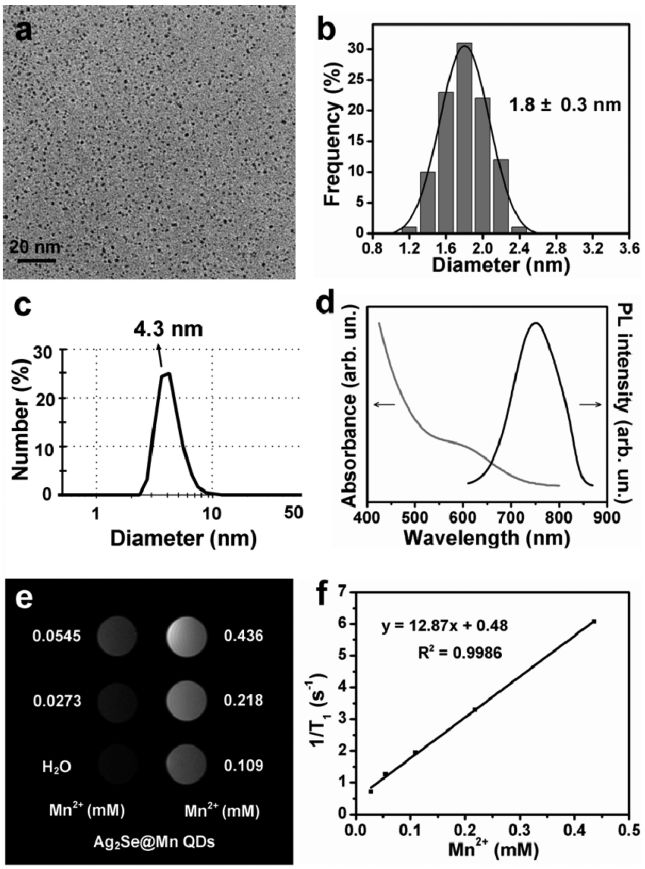

Figure 3. Characterization of the Ag_2Se@Mn QDs. (a) TEM image of the Ag_2Se@Mn QDs. (b) Average diameter of the Ag_2Se@Mn QDs analyzed based on the electron micrographs. (c) Hydrodynamic diameter of the Ag_2Se@Mn QDs detected by DLS. (d) UV–vis absorption and photoluminescence spectra of the Ag_2Se@Mn QDs. (e) T_1-weighted MR images of the Ag_2Se@Mn QDs at different concentrations of 0, 0.06 mg/mL, 0.12 mg/mL, 0.24 mg/mL, 0.48 mg/mL, and 0.96 mg/mL; the concentrations of Mn^{2+} converted from the corresponding concentration of the Ag_2Se@Mn QDs determined by ICP-AES. (f) Longitudinal relaxation rate ($1/T_1$) against the concentration of Mn^{2+} for the Ag_2Se@Mn QDs. The r_1 relaxivity, which is the slope of the curve, was calculated to be 12.87 mM^{-1} s^{-1}.

average size of 1.8 nm and a hydrodynamic diameter of 4.3 nm (Figure 3b,c). To the best of our knowledge, these QDs are by far the smallest NIR fluorescent-magnetic QDs.

The influence of the Mn^{2+} engineering on the optical properties of the Ag_2Se QDs was evaluated from UV–vis absorption and photoluminescence analysis. The photoluminescence spectrum of the Ag_2Se@Mn QDs showed an emission peak at 750 nm and the absorption spectrum exhibited a first excitonic transition peak at 585 nm (Figure 3d). Their absorption and emission peaks were the same as those of the host Ag_2Se QDs (Figure S4), indicating that the Mn^{2+} engineering had not altered the optical properties of the Ag_2Se QDs. However, after introduction of Mn^{2+}, the emission intensity of the Ag_2Se QDs was significantly improved, with an quantum yield of up to 13.2%, which might be attributed to the decrease in surface defects after surface bonding of Mn^{2+}.[38,39]

The MR imaging properties of the Ag_2Se@Mn QDs were investigated on a 7 T MR scanner at room temperature. The T1-weighted MR images of the Ag_2Se@Mn QDs in water exhibited a strong dependence of the signal intensity on the Ag_2Se@Mn QD concentration (Figure 3e). The longitudinal relaxivity (r_1) of the Ag_2Se@Mn QDs was measured to be 12.87 mM^{-1} s^{-1} at 7 T (Figure 3f), almost four times that of the commercial contrast agent Gd-DTPA (3.1 mM^{-1} s^{-1}).[40] Such a large relaxivity was mainly attributed to the accessibility of water to Mn^{2+} as a result of the surface localization of Mn^{2+} on the Ag_2Se@Mn QDs.

In addition to their ultrasmall size, strong NIR fluorescence and high longitudinal relaxivity, the Ag_2Se@Mn QDs do not contain any toxic heavy metal, thus they are relatively biocompatible. It was found that the Ag_2Se@Mn QDs had no cytotoxicity when incubated with CAL27 cells for 48 h at different concentrations of 0 to 200 μg/mL (Figure S5).

Instant and Efficient Labeling of MVs with the Ag_2Se@Mn QDs. Considering the increasing research interest in tumor-derived MVs, human oral squamous carcinoma (CAL27) cell-derived MVs were chosen as the model MVs for our labeling study. The MVs were separated and characterized according to our previous work (Figure S6).[7] The ultrasmall Ag_2Se@Mn QDs were directly loaded into the MVs by electroporation without any pretreatment. The entire labeling just included one step, which could be completed within several minutes. The electroporation changed neither the emission wavelength nor the intensity of the photoluminescence of the Ag_2Se@Mn QDs (Figure S7).

As shown in Figure 4a, the in situ HR-TEM image of the QDs in the MVs indicated that the lattice spacing (ca. 0.24 nm) was consistent with the distance between the adjacent (013) facets of Ag_2Se, demonstrating successful loading of the Ag_2Se@Mn QDs into the MVs by electroporation. As can be seen in Figure 4b, almost all the QD signals in the MVs pretreated by electroporation were colocalized with the signals of carboxyfluorescein diacetate succinimidyl ester (CFSE), a fluorescent dye commonly used for labeling MVs, but few QD signals could be observed in the MVs not pretreated by electroporation. The results of flow cytometric analysis also verified the efficient labeling of MVs with the Ag_2Se@Mn QDs (Figure 4c) because both the QD fluorescence intensity and the positive percentage of QD-labeled MVs were significantly higher in the MVs pretreated by electroporation than those in the MVs not pretreated. All these results showed that the labeling efficiency of our method is high.

To further demonstrate that our Ag_2Se@Mn QDs are agile enough to label the MVs and their ultrasmall size makes them quite compatible with the electroporation technique, we selected conventional water-dispersible CdSe/ZnS QDs with a relatively large size of 21.6 nm (Figure S8) in average hydrodynamic diameter, five times that of our Ag_2Se@Mn QDs (4.3 nm) and fluorescent doxorubicin (DOX), a small molecule cytotoxic drug to serve as the controls. Actually, DOX can be efficiently loaded into the extracellular vesicles by electroporation.[41] As illustrated in Figure 5a, the ultrasmall Ag_2Se@Mn QDs had an electroporation-mediated encapsulation efficiency of 27.5% (a mass ratio of the encapsulated materials to the initially added materials determined by ICP-AES and photoluminescence analyses), comparable to that of the DOX (29.1%). However, the large-sized CdSe/ZnS QDs had a low encapsulation efficiency of only 1.1%. These results suggested that the size is crucial for the successful loading of the QDs into the MVs by electroporation. A previous study has revealed that the instantaneously generated pores of the plasma membrane during electroporation are only ca. 1–10 nm in size.[30] The QDs are rigid, and thus only those smaller than the size of the pores can enter the MVs during electroporation. Our Ag_2Se@

DOI: 10.1021/jacs.5b10340
J. Am. Chem. Soc. 2016, 138, 1893–1903

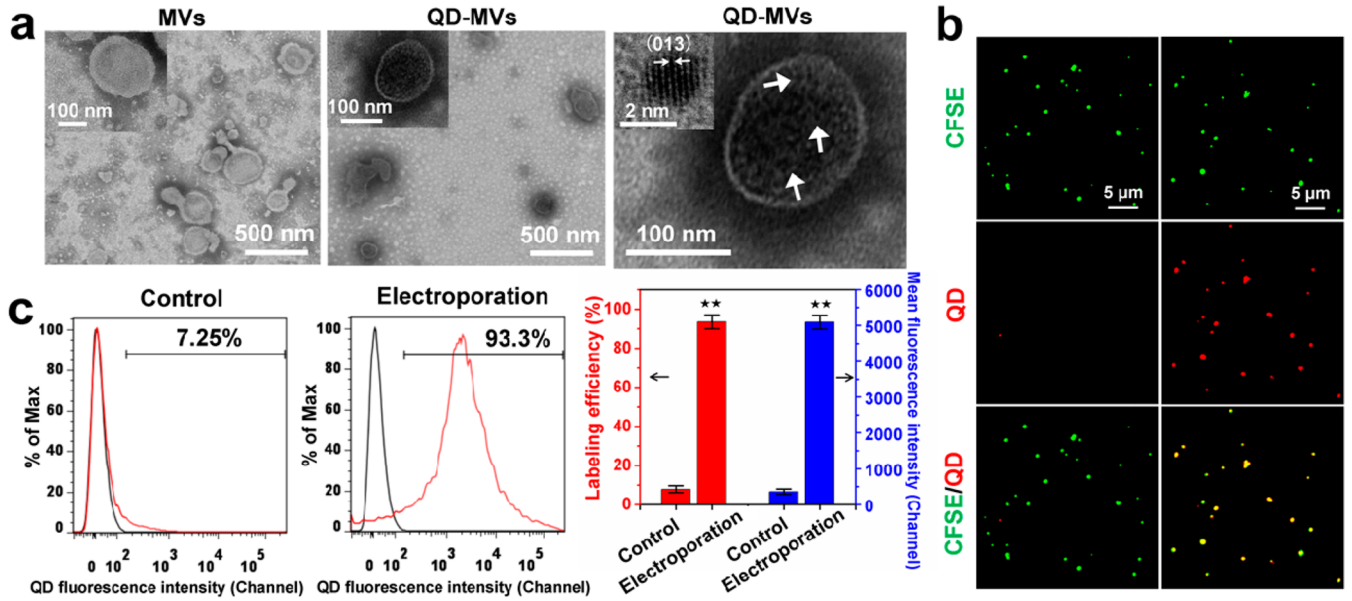

Figure 4. Ag_2Se@Mn QD labeling of the MVs with the assistance of electroporation. (a) TEM images of MVs before (MVs) and after (QD-MVs) electroporation with the Ag_2Se@Mn QDs, and in situ HR-TEM image of the QDs in the MVs. (b) Fluorescence images of CFSE-labeled MVs directly mixed (control, left) or electroporated (right) with the Ag_2Se@Mn QDs. (c) Flow cytometric histograms of MVs electroporated (red curve) or directly mixed (control, red curve) with the Ag_2Se@Mn QDs (left), and the quantified percentage of positively labeled MVs as well as the mean fluorescence intensity in each group (right), ★★, $P < 0.01$ versus the control group. The black curves in the flow cytometric histograms are the corresponding blank control, i.e., the MVs without any treatment.

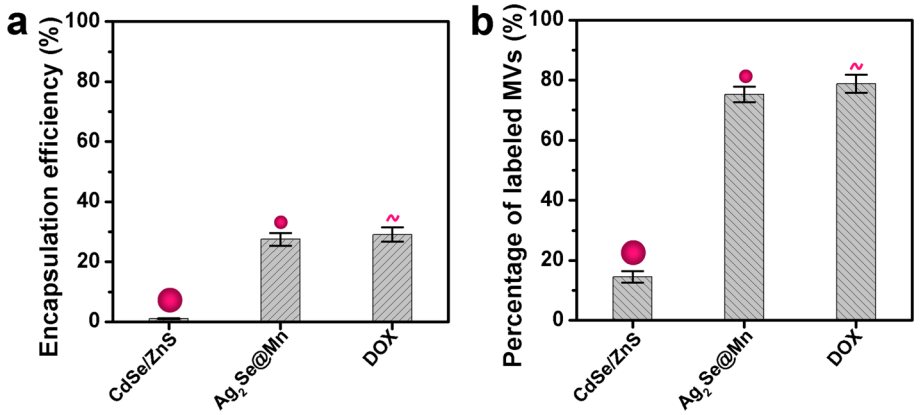

Figure 5. Electroporation-mediated loading efficiencies of the CdSe/ZnS QDs, Ag_2Se@Mn QDs and DOX into MVs. (a) Encapsulation efficiencies of the CdSe/ZnS QDs, Ag_2Se@Mn QDs, and DOX into MVs mediated by electroporation. (b) Percentage of positively labeled MVs after loading of the CdSe/ZnS QDs, Ag_2Se@Mn QDs and DOX by electroporation.

Mn QDs have an ultrasmall size of ca. 1.8 nm, with an average hydrodynamic diameter of only 4.3 nm. Therefore, they can fit with the electroporation technique. Accordingly, the flow cytometric analysis showed that the percentage of positively labeled MVs in the Ag_2Se@Mn QD-electroporation group was comparable to that in the DOX-electroporation group, and was much higher than that in the CdSe/ZnS QD-electroporation group (Figure 5b and Figure S8).

Besides the convenience and high efficiency, the proposed electroporation-mediated labeling of MVs with the Ag_2Se@Mn QDs is also controllable. By tuning the initial ratio of the Ag_2Se@Mn QDs to the MVs, the resulting fluorescence intensity of the QD-labeled MVs can be easily controlled (Figure S9), thus providing high feasibility of labeling MVs for different research purposes. Since one of the most attractive research interests in MVs is to exploit their therapeutic potentials, we then tested the compatibility of our electroporation-mediated strategy for QD labeling with therapeutic applications of MVs. The MVs were loaded simultaneously with the Ag_2Se@Mn QDs and the antitumor drug DOX by electroporation. The fluorescence colocalization and flow cytometric analyses showed that almost all the DOX signals were colocalized with the QD signals in the coelectroporated MVs. However, nearly no DOX or QD signals could be detected in the MVs not pretreated by electroporation. These results demonstrated that the Ag_2Se@Mn QDs and the DOX could be simultaneously and efficiently encapsulated into the MVs by electroporation (denoted as DOX-QD-MVs, Figure S10). Additionally, the Ag_2Se@Mn QDs did not influence the controllable loading of DOX into MVs. The dose of DOX in the MVs could be well controlled by adjusting the initial ratio of DOX to the MVs (Figure S11). DOX could be released from the DOX-QD-MVs to the target tumor cells and exhibited comparable cytotoxicity with that of the DOX-MVs (Figure

DOI: 10.1021/jacs.5b10340
J. Am. Chem. Soc. 2016, 138, 1893−1903

S12), indicating that the Ag_2Se@Mn QDs did not influence the cellular delivery of DOX by the MVs (Figure S13). These results demonstrated that the electroporation-mediated strategy for Ag_2Se@Mn QD labeling can well meet the demands from the study of MVs, e.g., simultaneously confer imaging and therapeutic functions on the MVs.

As can be seen from Table 1, the labeling strategy fit for MVs of diverse cellular origins, all of which had a comparable labeling efficiency of more than 90%. The width of the signal distribution revealed by the flow cytometric results further suggested that labeling with the Ag_2Se@Mn QDs could obtain a more homogeneously labeled population of MVs compared to labeling with dyes (Figure S14). All these results suggested that combination of the ultrasmall Ag_2Se@Mn QDs with the electroporation technique can realize instant efficient labeling of MVs, and the method is controllable, universal, and flexible.

Table 1. Electroporation-Mediated Ag_2Se@Mn QD Labeling Efficiencies of Diverse MVs

origin of MVs	labeling efficiency (%)	coefficient of variation (%)
CAL27	93.5	3.6
A549	92.7	3.4
MCF-7	92.9	4.1

Biocompatibility and Stability of the Ag_2Se@Mn QD-Labeled MVs. As mentioned above, good biocompatibility is essential for labeling and in vivo tracking of MVs. Since electroporation may potentially induce undesirable effects on the lipid bilayers of MVs, we therefore evaluated the influence of the electroporation-mediated Ag_2Se@Mn QD labeling on the intrinsic properties and functions of MVs. The results from dynamic light scattering (DLS) analysis showed that the average hydrodynamic diameter of the MVs after Ag_2Se@Mn QD labeling remained almost unchanged with 594.7 nm compared to 592.3 nm before labeling (Figure 6a). Besides, labeling with the Ag_2Se@Mn QDs caused very little change in the zeta potential of the MVs (Figure S15). Meanwhile, the flow cytometric analysis showed that the surface expression of phosphatidylserine (PS) and epithelial cell adhesion molecule (EpCAM), two characteristic markers of CAL27-derived MVs, was not significantly changed after labeling with the Ag_2Se@Mn QDs (Figure S16). Real-time quantitative polymerase chain reaction (qPCR) and Western blot analyses further indicated that labeling with the Ag_2Se@Mn QDs did not affect the mRNA or the protein expression of characteristic molecules in CAL27-derived MVs (Figure S17). The above results suggested that the properties and biochemical compositions of the MVs were well preserved after labeling with the Ag_2Se@Mn QDs via electroporation.

The uptake assay revealed that the internalization efficiency of the Ag_2Se@Mn QD-labeled MVs by the recipient cells was quite similar to that of the CFSE-labeled MVs (Figure 6b). Also, the results of methyl thiazolyl tetrazolium (MTT) assay showed that uptake of the Ag_2Se@Mn QD-labeled MVs did not influence the viability of the recipient cells, which was in line with the behaviors of the unlabeled control MVs (Figure 6c). These findings further confirmed that labeling with the Ag_2Se@Mn QDs had little influence on the intrinsic behaviors and functions of MVs.

The long-term real-time tracking of MVs needs labels to be able to emit stable detectable signal. Fortunately, the Ag_2Se@Mn QDs can resist photobleaching. Thus, Ag_2Se@Mn QD-labeled MVs could also resist photobleaching compared to the CFSE-labeled MVs (Figure 7a and Figure S18). Also, the Ag_2Se@Mn QD-labeled MVs exhibited excellent photostability in vivo. As shown in Figure S19a,b, after 60 min of continuous irradiation, the Ag_2Se@Mn QD-labeled MVs retained over 95% of their initial NIR fluorescence in vivo. Even at 72 h postinjection, there was still a significant NIR fluorescence

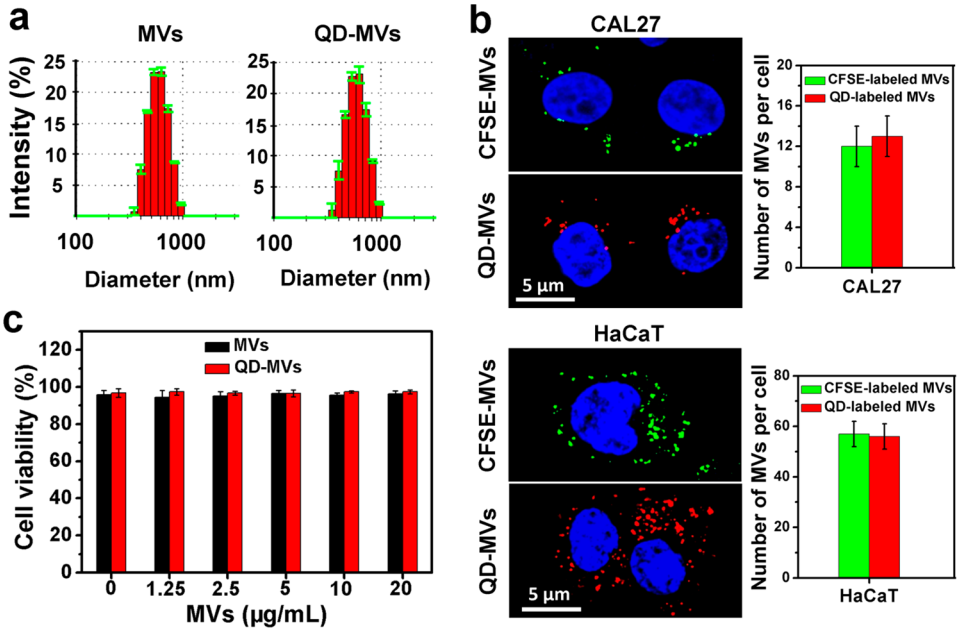

Figure 6. Effects of electroporation-mediated Ag_2Se@Mn QD labeling on MVs. (a) Hydrodynamic diameters of the MVs before (MVs) and after (QD-MVs) Ag_2Se@Mn QD labeling detected by DLS. (b) Fluorescence imaging and quantification for cellular uptake of CFSE- or Ag_2Se@Mn QD-labeled MVs by CAL27 and HaCaT cells after 2 h incubation. (c) Viability of CAL27 cells treated with increased concentrations (0–20 μg/mL) of unlabeled MVs (MVs) or Ag_2Se@Mn QD-labeled MVs (QD-MVs) for 48 h.

DOI: 10.1021/jacs.5b10340
J. Am. Chem. Soc. 2016, 138, 1893–1903

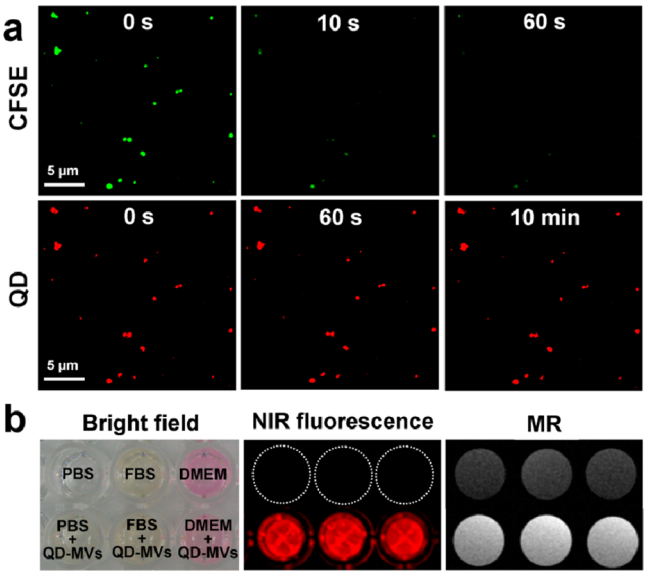

Figure 7. Signal stability of the Ag_2Se@Mn QD-labeled MVs. (a) Fluorescence images of CFSE- and Ag_2Se@Mn QD-labeled MVs under the continuous irradiation with a 488 nm laser. (b) Bright field, NIR fluorescence, and MR images of the Ag_2Se@Mn QD-labeled MVs dispersed in PBS, FBS, and DMEM.

(Figure S19c), characteristic of good in vivo signal stability of the Ag_2Se@Mn QD-labeled MVs. In addition, no significant decrease in QD signal was observed 7 days after storage of the Ag_2Se@Mn QD-labeled MVs at 4 °C (Figure S20). Besides, both the NIR fluorescence and MR signals of the Ag_2Se@Mn QD-labeled MVs were almost unchanged in different media (Figure 7b).

Whole-Body High-Resolution Dual-Mode Real-Time Tracking of MVs. Understanding the in vivo fate of MVs is crucial for assessing both the therapeutic efficacy and safety of MVs before their application in clinical trials. However, due to the current lack of sensitive imaging probes and adequate tracking techniques, the tissue distribution and clearance efficiency of MVs in vivo still remains poorly understood. Although recent studies have made attempts to monitor the in vivo biodistribution of MVs by multimodal imaging, the drawbacks of the imaging agents used and their imperfect combination with MVs have made whole-body high-resolution tracking of MVs very difficult in living animals in a long-term and real-time manner.[10,19] Here, by virtue of our labeling strategy using the Ag_2Se@Mn QDs, with some superiorities for tracking of MVs, and the high temporal resolution (100 ms) and high spatial resolution (297 μm) imaging achieved by the Ag_2Se@Mn QD labeling (Figure S21), we tried to monitor the in vivo dynamic biodistribution of MVs by simultaneous NIR fluorescence and MR imaging.

Continuous dual-mode tracking was carried out after intraperitoneal injection of the Ag_2Se@Mn QD-labeled MVs into the nude mice. As shown in Figure 8a, at 2 min postinjection of the Ag_2Se@Mn QD-labeled MVs, the NIR fluorescence signal was predominantly found in the peritoneal cavity. In addition, the NIR fluorescence of Ag_2Se@Mn QD-labeled MVs could also be detected on the dorsal side of the mouse (Figure S22a), suggesting a high fluorescence penetration depth of our Ag_2Se@Mn QDs (>1.0 cm). At 2–4 h postinjection, most of the Ag_2Se@Mn QD-labeled MVs appeared in the liver, spleen and kidneys as predominant NIR

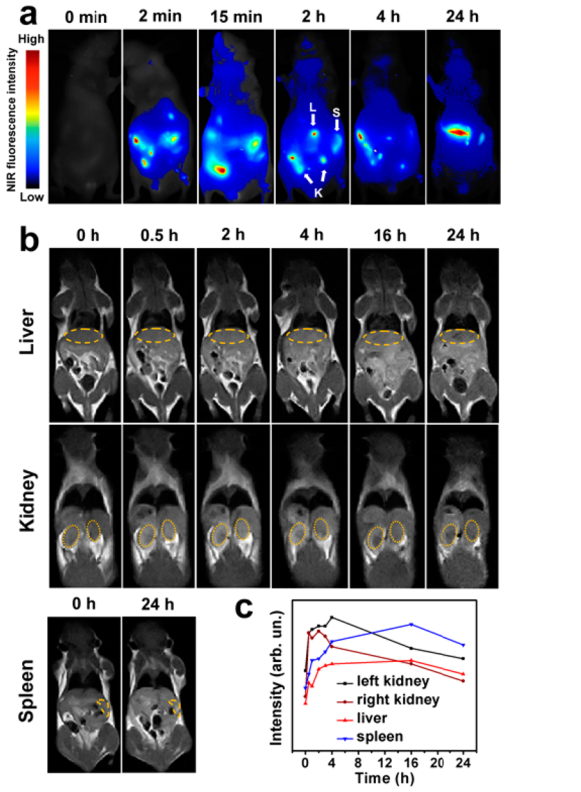

Figure 8. Whole-body dual-mode real-time tracking of the MVs. (a) NIR fluorescence images of nude mice collected at 0–24 h postinjection of the Ag_2Se@Mn QD-labeled MVs. L: liver, S: spleen, K: kidneys. (b) T_1-weighted images of mice liver, kidneys and spleen at 0–24 h postinjection of the Ag_2Se@Mn QD-labeled MVs. (c) Quantitative analysis of the T_1 signal intensity in mice liver, kidneys, and spleen after injection of the Ag_2Se@Mn QD-labeled MVs.

fluorescence signal was observed in these organs. The signal-to-background ratios of the NIR fluorescence signals in these organs were all above the Rose criterion of 5 (Figure S22b), indicating a positive detection of these organs by the NIR fluorescence imaging.[42] After 24 h, the Ag_2Se@Mn QD-labeled MVs were mainly retained in the liver and spleen, consistent with the ex vivo anatomical results (Figure S23).

The T_1-weighted MR imaging showed that there was a remarkable signal increase in the liver, spleen, and kidneys in the initial 4 h after intraperitoneal injection of the Ag_2Se@Mn QD-labeled MVs, and the maximum enhancement in these organs was 31%, 32%, and 48%, respectively (Figure 8b,c). Then, a notable signal decay in the kidneys and a slight increase followed by a significant decrease in the liver and spleen were observed. After 24 h, the signal in the kidneys almost subsided to the preinjection levels while there was still a signal enhancement of 23% in the liver and 30% in the spleen, suggesting remarkable accumulation of the Ag_2Se@Mn QD-labeled MVs in the liver and spleen, consistent with the NIR imaging results. On the basis of the above results, it can be seen that our labeling strategy using the advanced multifunctional Ag_2Se@Mn QDs not only can make the long-term whole-body dual-mode tracking of MVs realized in living animals with both high sensitivity and high resolution, but also revealed the in vivo dynamic biodistribution of MVs in a real-time and in situ quantitative manner.

DOI: 10.1021/jacs.5b10340
J. Am. Chem. Soc. 2016, 138, 1893–1903

CONCLUSIONS

In summary, based on our previously reported ultrasmall Ag_2Se QDs and a newly developed method for controllable surface localization of Mn^{2+}, nontoxic Ag_2Se@Mn QDs have been fabricated, with an ultrasmall size of ca. 1.8 nm, water dispersibility, high NIR fluorescence quantum yield of 13.2% and high longitudinal relaxivity of 12.87 mM^{-1} s^{-1}. By coupling the ultrasmall Ag_2Se@Mn QDs with the electroporation technique, the instant and efficient labeling of MVs has been achieved, capable of conferring both NIR fluorescence and MR traceability on MVs. Compared to existing strategies for labeling MVs, our one-step conjugation-free labeling strategy does not need any pretreatment, chemical modification or genetic engineering for the MVs or their donor cells, and hence it is time- and labor-saving, and user- and biofriendly. Meanwhile, such a labeling strategy is of universality for MVs of different origins without unfavorable influence on inherent behaviors of MVs. In addition, the electroporation-mediated Ag_2Se@Mn QD labeling is controllable and flexible. By virtue of the complementary NIR fluorescence and MR imaging capabilities of the Ag_2Se@Mn QDs, the whole-body high-resolution dual-mode tracking of MVs in vivo can be realized and can be used to reveal the dynamic biodistribution of MVs in a real-time and in situ quantitative manner. Overall, this study not only opens a new window for QD-based nanotechnology, but also facilitates the investigation and application of MVs.

EXPERIMENTAL SECTION

Reagents and Instruments. Reduced glutathione (GSH) and L-alanine (Ala, 98.5%) were purchased from Amresco. Sodium selenite (Na_2SeO_3, 97%), silver nitrate ($AgNO_3$, 99%), and $Mn(NO_3)_2$ (99%) were obtained from Sinopharm Chemical Reagent Co., Ltd. Yeast glutathione reductase (GR, ≥ 100 unites/mg protein) was bought from Calbiochem. Reduced β-nicotinamide adenine dinucleotide 2′-phosphate tetrasodium salt (NADPH) was purchased from Roche. Electroporation buffer was bought from Bio-Rad Corp. Carboxyfluorescein diacetate succinimidyl ester (CFSE) and primary antibodies against epithelial cell adhesion molecule (EpCAM) were purchased from Sigma-Aldrich. Hoechst 33342 was bought from Invitrogen. Fluorochrome-labeled antibodies for flow cytometry including Annexin V-FITC, EpCAM-Cy3, as well as corresponding isotype controls were bought from BD Biosciences. BCA protein assay kit was purchased from Beyotime Institute of Biotechnology. Primary antibodies against endothelial growth factor receptor (EGFR) were purchased from Epitomics. Primary antibodies against β-Actin were obtained from Santa Cruz. Ultrapure water (18 MΩ·cm) was made by a Millipore Milli-Q system.

UV−vis absorption spectra and fluorescence spectra were collected on a Shimadzu UV-2550 spectrometer and a Horiba Jobin Yvon Inc. Fluorolog-3 spectrophotometer, respectively. Element contents were measured on a Spectro Genesis ICP-AES spectrometer. STEM was performed on an atomic resolution analytical microscope (JEM-ARM 200F) operating at 200 kV. STEM-EDX elemental mapping was also performed on JEM-ARM 200F. HR-TEM images were obtained on a JEOL JEM-2100 transmission electron microscope (200 kV). XPS spectra were recorded using a VG Multilab 2000 X-ray photoelectron spectrometer. EPR spectrum was collected on a Bruker X-band A200 spectrometer (9.4 GHz) at a temperature of 110 K. DLS measurements were performed on a Malvern Zetasizer Nano ZS instrument. Relaxation times measurements and in vitro MR imaging were performed on a 7 T Bruker Biospec Avance spectrometer. The imaging parameters were set as follows: repetition time (TR) = 300 ms; echo time (TE) = 11 ms; field of view (FOV) = 3.5 × 3.0 cm^2; and slice thickness = 1 mm.

Fabrication of the Ag_2Se@Mn QDs. The host Ag_2Se QDs were synthesized according to our previous report and the whole process was carried out under Ar atmosphere.[33] In a typical preparation, $AgNO_3$ (18.0 μmol) and Ala (22.5 μmol) were added to 18 mL of NaOH solution (0.1 M) to obtain the silver precursor. The selenium precursor was prepared by successively adding GSH (14.4 μmol), Na_2SeO_3 (3.6 μmol), NADPH (3.6 μmol), and GR (14.6 μL) to 12 mL of BR buffer (pH 7.1) at room temperature. Then the selenium precursor was immediately injected into the reaction flask of silver precursor solution, and the mixture was vigorously stirred at 90 °C for 10 s. The as-prepared Ag_2Se QDs were quickly cooled in an ice bath and purified via ultrafiltration (MWCO 10 kDa).

The surface composition of the Ag_2Se QDs was tuned by heating them in NaOH solution (0.1 M) at 80 °C under stirring. After determination of the most appropriate amount of Ag_2O using XPS analysis, the heating time of 10 min was selected for the subsequent preparation of the Ag_2Se@Mn QDs.

After the above treatment, the Ag_2Se@Mn QDs were prepared by dropwise adding $Mn(NO_3)_2$ (10 mM) to the surface-engineered Ag_2Se QDs solution (~0.25 mg/mL) at room temperature under stirring. The QD solution was stored at 4 °C for 24 h and then the obtained Ag_2Se@Mn QDs were purified via ultrafiltration (MWCO 10 kDa) and dialysis (MWCO 3500) for the following applications.

Cell Culture and MV Purification. Human oral squamous cell carcinoma (CAL27) cells, human lung epithelial carcinoma (A549) cells, human breast cancer (MCF-7) cells, and human immortalized noncancerous keratinocytes (HaCaT) cells were purchased from China Center for Type Culture Collection. They were cultured in Dulbecco's Modified Eagle Medium (DMEM, Gibco) supplemented with 10% (v/v) fetal bovine serum (FBS), 1% (v/v) penicillin, and 1% (v/v) streptomycin at 37 °C in a 5% CO_2-humidified environment.

MVs were purified from the supernatants of starved cells according to our previous description.[7] First, cells were cultured in serum-free medium for 48 h to allow the release of MVs. Subsequently, the culture medium was collected and centrifuged (2000*g* for 15 min) to remove the dead cells and cell debris. The resulting supernatants were then centrifuged at 50 000*g* for 60 min to isolate and concentrate MVs. The isolated MVs were washed with sterile PBS and further purified by centrifugation at 50 000*g* for 60 min again. The obtained MVs were resuspended in sterile PBS and stored at −80 °C for further use. All the isolation and purification procedures were carried out at 4 °C. To determine the amount of the obtained MVs, their total protein content was quantified by BCA protein assay.

Electroporation-Mediated Ag_2Se@Mn QD Labeling of MVs. To label the MVs with the Ag_2Se@Mn QDs, MVs (125 μg, protein content), increased amounts of Ag_2Se@Mn QDs and electroporation buffer (250 μL) were mixed in 0.4 cm electroporation cuvettes. After electroporation at 250 V and 350 μF on an electroporation system (Bio-Rad Gene Pulser Xcell), the mixture was incubated for 30 min at 37 °C to allow the recovery of the membrane of the MVs. The excess Ag_2Se@Mn QDs were separated from MVs by sucrose density gradient centrifugation (15%−60%). After determination of the most appropriate loading efficiency using flow cytometric analysis, the concentration of 0.2 mg/mL for the Ag_2Se@Mn QDs were selected for the subsequent analysis and studies.

Characterization and Analysis of the Ag_2Se@Mn QD-Labeled MVs. For TEM characterization, the MVs suspended in PBS were dropped onto a carbon-coated copper grid and negatively stained with 1% phosphotungstic acid. Samples were then examined on a transmission electron microscope (Hitachi HT7700). The in situ HR-TEM samples were prepared by drying the Ag_2Se@Mn QD-labeled MVs on a copper grid coated with ultrathin carbon film and examined on a high resolution transmission electron microscope (JEOL JEM-2100).

For fluorescence colocalization analysis, the CFSE-labeled MVs were electroporated with the Ag_2Se@Mn QDs to obtain CFSE and QD dual-labeled MVs. The fluorescence images were obtained on a laser confocal fluorescence microscope (Nikon A1MP STORM). CFSE and QDs were excited by using a laser at 488 nm, and their fluorescence signals were separated by using different filters. To

DOI: 10.1021/jacs.5b10340
J. Am. Chem. Soc. 2016, 138, 1893−1903

inspect the photostability of the labeling materials, the CFSE- and Ag_2Se@Mn QD-labeled MVs were irradiated continuously with a 488 nm laser on the confocal microscope, and the fluorescence images were acquired with 5 s intervals.

Flow cytometric analysis was carried out on BD FACSAria III. The flow cytometric analysis was performed to assess the labeling efficiency of MVs with the Ag_2Se@Mn QDs.

To compare the electroporation-mediated encapsulation efficiency of the Ag_2Se@Mn QDs with that of the CdSe/ZnS QDs and that of the DOX, MVs were electroporated with the CdSe/ZnS QDs and the DOX under the same conditions used for the Ag_2Se@Mn QDs, as described above. The initial concentrations of the QDs (or DOX) and the MVs for all the groups were 0.025 and 0.5 mg/mL (protein content), respectively. The encapsulation efficiency of the QDs was evaluated by ICP-AES analysis and that of the DOX was assessed by detecting the intrinsic fluorescence of DOX using a Horiba Jobin Yvon Inc. Fluorolog-3 spectrophotometer.

The hydrodynamic diameters of the MVs were characterized using a zetasizer instrument (Malvern Nano-ZS ZEN 3600).

The viability of CAL27 cells after incubation with increased concentrations of the Ag_2Se@Mn QD-labeled MVs for 48 h was measured using a cell viability analyzer (Beckman coulter).

To investigate and compare the cellular internalization of the Ag_2Se@Mn QD- and CFSE-labeled MVs, uptake assays using CAL27 cells and HaCaT cells as the recipient cells were carried out. Cells were cultured in a 3.5 cm glass bottomed Petri dish for 24 h and then incubated with Ag_2Se@Mn QD- or CFSE-labeled MVs (20 μg/mL) for 2 h at 37 °C. After the incubation, the fluorescence images were obtained on the laser confocal fluorescence microscope.

To assess the NIR fluorescence and MR imaging capabilities of the Ag_2Se@Mn QD-labeled MVs and their stability in different media, Ag_2Se@Mn QD-labeled MVs were dispersed in PBS, FBS and DMEM, and then subjected to an in vivo fluorescence imaging system (CRi Maestro) and an in vivo MR imaging system (Bruker Biospec Avance) to acquire NIR fluorescence and MR images, respectively. The NIR images were analyzed using the Maestro 3.0 software and the MR images were analyzed using the ImageJ software.

In Vivo Dual-Mode Tracking of MVs. Female nude Balb/c mice (6-week-old) were obtained from Hunan SJA Laboratory Animal Co., Ltd. and raised in an animal facility under filtered air. Animal studies were performed under the guidelines approved by the Animal Care and Use Committee of Wuhan University.

To monitor the in vivo dynamic biodistribution of MVs, Ag_2Se@Mn QD-labeled MVs (200 μg) were injected intraperitoneally to mice. Then the mice were subjected to an in vivo fluorescence imaging system (CRi Maestro) and an in vivo MR imaging system (Niumag MesoMR). A series of images were acquired at scheduled time intervals. The NIR images were analyzed using the Maestro 3.0 software. To quantify the biodistribution of the MVs in mice, the average signal intensity of the regions of interest (liver, kidney, and spleen) in the MR images was quantified using the ImageJ software.

■ ASSOCIATED CONTENT

Supporting Information

The Supporting Information is available free of charge on the ACS Publications website at DOI: 10.1021/jacs.5b10340.

Additional experimental details and figures (PDF)

■ AUTHOR INFORMATION

Corresponding Author

*dwpang@whu.edu.cn

Author Contributions

J.-Y.Z. and G.C. contributed equally to this work.

Notes

The authors declare no competing financial interest.

■ ACKNOWLEDGMENTS

This work was supported by the National Basic Research Program of China (973 Program, 2011CB933600), the National Natural Science Foundation of China (21535005 and 81300895), the 111 Project (111-2-10), and Collaborative Innovation Center for Chemistry and Molecular Medicine. We thank Prof. Si-Shen Xie, Prof. Lin Gu and Mr. Xin-An Yang from the Institute of Physics, Chinese Academy of Sciences for their help with the scanning transmission electron microscopy.

■ REFERENCES

(1) Cocucci, E.; Racchetti, G.; Meldolesi, J. *Trends Cell Biol.* **2009**, *19*, 43.
(2) Raposo, G.; Stoorvogel, W. *J. Cell Biol.* **2013**, *200*, 373.
(3) Camussi, G.; Deregibus, M. C.; Bruno, S.; Cantaluppi, V.; Biancone, L. *Kidney Int.* **2010**, *78*, 838.
(4) Robbins, P. D.; Morelli, A. E. *Nat. Rev. Immunol.* **2014**, *14*, 195.
(5) Gatti, S.; Bruno, S.; Deregibus, M. C.; Sordi, A.; Cantaluppi, V.; Tetta, C.; Camussi, G. *Nephrol., Dial., Transplant.* **2011**, *26*, 1474.
(6) Al-Nedawi, K.; Meehan, B.; Micallef, J.; Lhotak, V.; May, L.; Guha, A.; Rak, J. *Nat. Cell Biol.* **2008**, *10*, 619.
(7) Chen, G.; Zhu, J. Y.; Zhang, Z. L.; Zhang, W.; Ren, J. G.; Wu, M.; Hong, Z. Y.; Lv, C.; Pang, D. W.; Zhao, Y. F. *Angew. Chem., Int. Ed.* **2015**, *54*, 1036.
(8) Zhang, Y. Q.; Li, L. M.; Yu, J. X.; Zhu, D. H.; Zhang, Y. J.; Li, X. H.; Gu, H. W.; Zhang, C. Y.; Zen, K. *Biomaterials* **2014**, *35*, 4390.
(9) Tang, K.; Zhang, Y.; Zhang, H. F.; Xu, P. W.; Liu, J.; Ma, J. W.; Lv, M.; Li, D. P.; Katirai, F.; Shen, G. X.; Zhang, G. M.; Feng, Z. H.; Ye, D. Y.; Huang, B. *Nat. Commun.* **2012**, *3*.
(10) Silva, A. K. A.; Kolosnjaj-Tabi, J.; Bonneau, S.; Marangon, I.; Boggetto, N.; Aubertin, K.; Clement, O.; Bureau, M. F.; Luciani, N.; Gazeau, F.; Wilhelm, C. *ACS Nano* **2013**, *7*, 4954.
(11) Vader, P.; Breakefield, X. O.; Wood, M. J. A. *Trends Mol. Med.* **2014**, *20*, 385.
(12) Gyorgy, B.; Hung, M. E.; Breakefield, X. O.; Leonard, J. N. *Annu. Rev. Pharmacol. Toxicol.* **2015**, *55*, 439.
(13) van der Vlist, E. J.; Nolte-'t Hoen, E. N. M.; Stoorvogel, W.; Arkesteijn, G. J. A.; Wauben, M. H. M. *Nat. Protoc.* **2012**, *7*, 1311.
(14) Nabhan, J. F.; Hu, R. X.; Oh, R. S.; Cohen, S. N.; Lu, Q. *Proc. Natl. Acad. Sci. U. S. A.* **2012**, *109*, 4146.
(15) Silva, A. K. A.; Di Corato, R.; Pellegrino, T.; Chat, S.; Pugliese, G.; Luciani, N.; Gazeau, F.; Wilhelm, C. *Nanoscale* **2013**, *5*, 11374.
(16) Musa, S. M. *Nanoscale Flow: Advances, Modeling, and Applications*; CRC Press: Boca Raton, FL, 2014.
(17) Louie, A. Y. *Chem. Rev.* **2010**, *110*, 3146.
(18) Lee, D. E.; Koo, H.; Sun, I. C.; Ryu, J. H.; Kim, K.; Kwon, I. C. *Chem. Soc. Rev.* **2012**, *41*, 2656.
(19) Lai, C. P.; Mardini, O.; Ericsson, M.; Prabhakar, S.; Maguire, C. A.; Chen, J. W.; Tannous, B. A.; Breakefield, X. O. *ACS Nano* **2014**, *8*, 483.
(20) Resch-Genger, U.; Grabolle, M.; Cavaliere-Jaricot, S.; Nitschke, R.; Nann, T. *Nat. Methods* **2008**, *5*, 763.
(21) Kheirolomoom, A.; Kruse, D. E.; Qin, S. P.; Watson, K. E.; Lai, C. Y.; Young, L. J. T.; Cardiff, R. D.; Ferrara, K. W. *J. Controlled Release* **2010**, *141*, 128.
(22) Weissleder, R. *Nat. Biotechnol.* **2001**, *19*, 316.
(23) Frangioni, J. V. *Curr. Opin. Chem. Biol.* **2003**, *7*, 626.
(24) Bashkatov, A. N.; Genina, E. A.; Kochubey, V. I.; Tuchin, V. V. *J. Phys. D: Appl. Phys.* **2005**, *38*, 2543.
(25) Jiang, P.; Zhu, C. N.; Zhang, Z. L.; Tian, Z. Q.; Pang, D. W. *Biomaterials* **2012**, *33*, 5130.
(26) Shen, S. L.; Wang, Q. B. *Chem. Mater.* **2013**, *25*, 1166.
(27) Dong, B. H.; Li, C. Y.; Chen, G. C.; Zhang, Y. J.; Zhang, Y.; Deng, M. J.; Wang, Q. B. *Chem. Mater.* **2013**, *25*, 2503.
(28) Hu, F.; Li, C. Y.; Zhang, Y. J.; Wang, M.; Wu, D. M.; Wang, Q. B. *Nano Res.* **2015**, *8*, 1637.
(29) Weissleder, R.; Pittet, M. J. *Nature* **2008**, *452*, 580.

DOI: 10.1021/jacs.5b10340
J. Am. Chem. Soc. 2016, 138, 1893−1903

(30) Tsong, T. Y. *Biophys. J.* **1991**, *60*, 297.
(31) Yarmush, M. L.; Golberg, A.; Sersa, G.; Kotnik, T.; Miklavcic, D. *Annu. Rev. Biomed. Eng.* **2014**, *16*, 295.
(32) Alvarez-Erviti, L.; Seow, Y. Q.; Yin, H. F.; Betts, C.; Lakhal, S.; Wood, M. J. A. *Nat. Biotechnol.* **2011**, *29*, 341.
(33) Gu, Y. P.; Cui, R.; Zhang, Z. L.; Xie, Z. X.; Pang, D. W. *J. Am. Chem. Soc.* **2012**, *134*, 79.
(34) Jing, L. H.; Ding, K.; Kershaw, S. V.; Kempson, I. M.; Rogach, A. L.; Gao, M. Y. *Adv. Mater.* **2014**, *26*, 6367.
(35) Shen, S. L.; Zhang, Y. J.; Liu, Y. S.; Peng, L.; Chen, X. Y.; Wang, Q. B. *Chem. Mater.* **2012**, *24*, 2407.
(36) Mikulec, F. V.; Kuno, M.; Bennati, M.; Hall, D. A.; Griffin, R. G.; Bawendi, M. G. *J. Am. Chem. Soc.* **2000**, *122*, 2532.
(37) Bose, R.; Manna, G.; Pradhan, N. *J. Phys. Chem. C* **2013**, *117*, 20991.
(38) Smith, A. M.; Nie, S. M. *Acc. Chem. Res.* **2010**, *43*, 190.
(39) Kim, J. Y.; Voznyy, O.; Zhitomirsky, D.; Sargent, E. H. *Adv. Mater.* **2013**, *25*, 4986.
(40) Kalavagunta, C.; Michaeli, S.; Metzger, G. J. *Contrast Media Mol. Imaging* **2014**, *9*, 169.
(41) Tian, Y. H.; Li, S. P.; Song, J.; Ji, T. J.; Zhu, M. T.; Anderson, G. J.; Wei, J. Y.; Nie, G. J. *Biomaterials* **2014**, *35*, 2383.
(42) Bushberg, J. T. *The Essential Physics of Medical Imaging*; Lippincott Williams & Wilkins: Baltimore, 2002.

DOI: 10.1021/jacs.5b10340
J. Am. Chem. Soc. 2016, 138, 1893−1903